Inelastic Neutron Scattering Investigation in Glassy SiSe2: Complex Dynamics at the Atomic Scale

ARTICLE *in* JOURNAL OF PHYSICAL CHEMISTRY LETTERS · MARCH 2013

Impact Factor: 7.46 · DOI: 10.1021/jz400232c

5 AUTHORS, INCLUDING:

Marco Zanatta
Università degli Studi di Perugia
14 PUBLICATIONS **95** CITATIONS
SEE PROFILE

Andrea Orecchini
Università degli Studi di Perugia
64 PUBLICATIONS **442** CITATIONS
SEE PROFILE

THE JOURNAL OF PHYSICAL CHEMISTRY Letters

Letter

pubs.acs.org/JPCL

Inelastic Neutron Scattering Investigation in Glassy $SiSe_2$: Complex Dynamics at the Atomic Scale

Marco Zanatta,*[,†] A. Fontana,[‡,¶] A. Orecchini,[†,§,∥] C. Petrillo,[†,§] and F. Sacchetti[†,§]

[†]Dipartimento di Fisica and [§]IOM CNR c/o Dipartimento di Fisica, Università di Perugia, I-06123 Perugia, Italy

[‡]Dipartimento di Fisica, Università di Trento, I-38050 Povo, Trento, Italy

[¶]IPCF CNR, UOS di Roma, c/o Università di Roma "La Sapienza", I-00185 Roma, Italy

[∥]Institut Laue Langevin, F-38042 Grenoble, France

ABSTRACT: A detailed investigation of the THz dynamics in glassy $SiSe_2$ by means of neutron inelastic scattering is presented. To carefully map the translational dynamics and the region of the boson peak, we carried out two different experiments with sharp and broad resolutions coupled with a narrow and a wide kinematic range, respectively. Data show a complex pattern of excitations made up of three components. The most intense one is the prolongation of the longitudinal acoustic mode while two other modes appear in the boson peak region below 3 meV. We propose an interaction model that allows for a consistent identification of the nature of these modes.

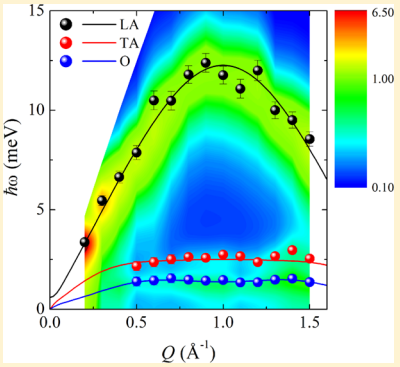

SECTION: Glasses, Colloids, Polymers, and Soft Matter

Disordered solids constitute a class of materials with widespread applications in everyday life. Glasses, polymers, colloids, and biological systems, such as proteins, are all characterized by the presence of topological disorder. Moreover, despite a large spectrum of different chemical and physical properties, all of these systems share some common properties that are intimately related to their disordered structure. A striking example is the so-called boson peak (BP), a broad peak universally visible in the reduced vibrational density of states $g(\omega)/\omega^2$ of disordered systems.[1−3] The origin of this feature is still a debated topic,[4−7] but it is deeply connected to the disorder dependence of the vibrational dynamics.[8,9]

Glasses, and in particular network glasses, usually formed by few atomic species, are among the simplest case studies. Their structure, although lacking long-range order, is far from being stochastic.[10] In particular, atomic glasses form short-range crystal-like structures that retain a certain degree of order beyond the first neighbors scale. In the macroscopic regime, that is, when the wavelength λ of an external probe is much larger than the typical interatomic spacing, network details can be neglected, and glasses behave like an elastic continuum. In this region, glasses support sound waves as crystals do. Decreasing the length scale to a few nanometers, the continuum approximation breaks down, and acoustic excitations evolve toward a more complex pattern of vibrations. Experimentally, this region is accessible by means of inelastic neutron scattering (INS) and inelastic X-ray scattering (IXS) as well as by numerical simulations; see refs 11−20. The observable is the so-called dynamic structure factor $S(Q,\omega)$, the space and time Fourier transform of the density−density correlation function. IXS and INS experiments on v-SiO_2,[15,18] v-GeO_2,[16] and v-$GeSe_2$[19] report on a high-frequency mode that is considered the evolution of the longitudinal acoustic vibrations. Spectra show a broad peak whose energy follows a phonon-like pseudoperiodic sinusoidal dispersion. The periodicity is defined by the position Q_1 of the first sharp diffraction peak in the static structure factor $S(Q)$. The maximum of the dispersion is located at $Q_m \approx Q_1/2$, which acts like the boundary of a Brillouin zone. Very accurate investigations have shown that in prototypical systems, an additional low-energy branch appears as an almost Q-independent mode close to the very intense elastic line.[15,16,19] Computational works suggest a transverse acoustic nature for this mode, which is heavily affected by the disorder and is visible through a mixing of modes.[14]

In this Letter, we present an extended INS investigation of the glassy system $SiSe_2$, whose structure is based on $SiSe_4$ tetrahedra that are linked in a mostly edge-sharing way.[22−24] $SiSe_2$ is a coherent neutron scatterer characterized by a rather low sound velocity (∼1700 m/s) so that it is an ideal candidate for INS investigations. As suggested in refs 16 and 19, to map out all of the relevant dynamic features, we performed two different experiments at the spectrometers BRISP (Institut

Received: January 31, 2013
Accepted: March 15, 2013

   dx.doi.org/10.1021/jz400232c | *J. Phys. Chem. Lett.* 2013, 4, 1143−1147

Laue Langevin, Grenoble, France),[25,26] and TOFTOF (FRM-II, Münich, Germany).[27] These experiments reveal a complex dynamics of $SiSe_2$ at the atomic scale, showing the existence of three distinct modes.

The experimental approach is outlined in Figure 1, which shows the $(\hbar\omega,Q)$ kinematic regions investigated and the instrumental resolutions (see details in the Experimental Methods section). The scattering intensities are shown in Figure 2 at typical Q values for both BRISP (left column) and TOFTOF (central column). The single scattering intensity can be written as

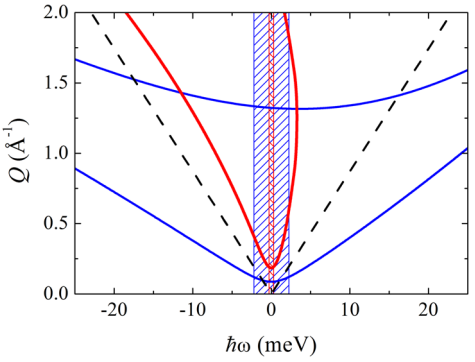

Figure 1. BRISP (blue line) and TOFTOF (red line) kinematic ranges. The shaded regions represent the full width at half-maximum (fwhm) of the instrumental resolutions. The high-frequency extrapolation of the longitudinal sound velocity measured by Brillouin light scattering is also reported (dashed black line); v_L^0 = 1740 m/s[21].

$$I(Q,\omega) = K_i R_i(\omega) \otimes S(Q,\omega)\beta\omega[n(\omega)+1] \quad (1)$$

where $n(\omega)$ is the Bose factor and β the inverse temperature. $R_i(\omega)$ is the instrument resolution, and K_i an instrument scale parameter.

A meticulous spectral shape analysis was carried out to identify the various inelastic components present in our spectra. BRISP data show the existence of a mode, j_1, lying at rather high energy; see Figure 2a and d. On the other hand, TOFTOF data show a peak very close to the elastic line, Figure 2b and e. The $S(Q,\omega)$ in eq 1 has to describe both BRISP and TOFTOF data; consequently, the inelastic scattering was first modeled as the sum of two damped harmonic oscillators (DHO). However, this model does not fit properly the low-energy features. A good agreement is obtained when two low-energy components j_2 and j_3 are introduced. Because j_2 and j_3 are very close in energy, the most general description should consider also the interaction between them. The interaction of j_1 can be neglected by considering that, in the experimental Q range, it has an energy that largely exceeds those of j_2 and j_3, thus allowing one to simplify the scheme. It is worth recalling that a similar approach with interacting modes was already employed in ref 6.

According to these observations and assuming a δ function for the elastic peak, $S(Q,\omega)$ was modeled by the sum of a DHO, representing j_1, and the dynamic structure factor of a system of two interacting oscillators for j_2 and j_3. The Hamiltonian of the system is thus given by

$$\mathcal{H} = \mathcal{H}_o + \frac{1}{2}\sum_{\mathbf{Q}} U(Q)[\mathbb{Q}^\dagger_{Q\,j_2}\mathbb{Q}_{Q\,j_3} + \mathbb{Q}^\dagger_{Q\,j_3}\mathbb{Q}_{Q\,j_2}] + \mathcal{H}_a \quad (2)$$

where $\mathcal{H}_o = (1/2)\sum_{\mathbf{Q}j_k}[\mathbb{P}^\dagger_{Q\,j_k}\mathbb{P}_{Q\,j_k} + \omega^2_{Q\,j_k}\mathbb{Q}^\dagger_{Q\,j_k}\mathbb{Q}_{Q\,j_k}]$, with k = 1−3. $\mathbb{P}_{Q\,j_k}$ and $\mathbb{Q}_{Q\,j_k}$ are the momentum and coordinate of the j_k oscillator. $U(Q)$ is the coupling parameter between j_2 and j_3 and $\mathcal{H}_a$ contains the higher-order components. Following refs 28 and 29, the diagonal Green's function $G_{j_kj_k}(Q,\omega)$ for the interacting oscillators j_2 and j_3 is obtained from the equation of motion, that is

$$G_{j_kj_k}(Q,\omega) = \frac{1}{2\pi}\frac{\chi_{j_k}(Q,\omega)}{1-\chi_{j_k}(Q,\omega)\chi_{j_{k'}}(Q,\omega)|U(Q)|^2} \quad (3)$$

where $\chi_{j_k}(Q,\omega) = [\omega^2 - \omega^2_{Q\,j_k} - \sum_{j_k}(Q,\omega)]^{-1}$, $j_k \neq j_{k'}$. Self-energies due to $\mathcal{H}_a$ are approximated as $\sum_{j_k}(Q,\omega) = i\omega\Gamma_{j_k}(Q)$,

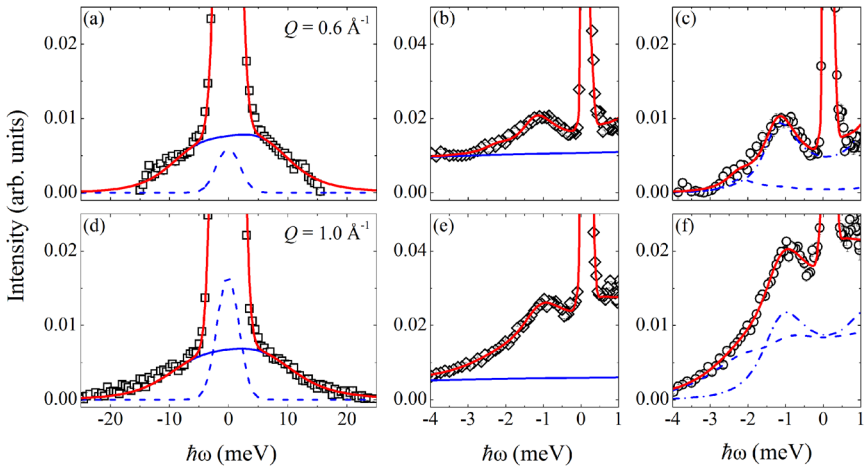

Figure 2. Experimental data at two typical Q values, Q = 0.6 (first row) and 1.0 Å^{-1} (second row). The red line represents the best fit to the data (see text). The left column reports BRISP spectra (black open squares); blue lines are the fit components, j_1 (solid blue line) and the sum of j_2 and j_3 (dashed blue line). TOFTOF data are reported in the central column (black open diamonds); the solid blue line is j_1 as derived from the fit of BRISP data. Open black circles in the right column show TOFTOF spectra after the subtraction of j_1 (solid blue line in panels (b) and (e)). The blue dashed line and the blue dashed−dotted line represent j_2 and j_3, respectively (see text). Notice the energy scale of the BRISP data with respect to that of the TOFTOF spectra.

dx.doi.org/10.1021/jz400232c | J. Phys. Chem. Lett. 2013, 4, 1143−1147

where $\Gamma_{j_k}(Q)$ is the damping of the j_k mode. We assume that coupling between the modes must have a finite interaction range in the real space. This implies that the Fourier transform of $U(Q)$ has a finite $\langle r^2 \rangle$. Consequently, we chose a simple form for $U(Q)$, writing it as a fast-decaying exponential function, that is $U(Q) = U_0 Q \exp[-R^2Q^2]$, with U_0 and R^2 constants. It is worth noticing that other approximations, such as a simple exponential, produce an infinite range in real space. Neglecting off-diagonal terms, the imaginary part of $G_{j_k j_k}(Q,\omega)$ is proportional to the $S(Q,\omega)$ of the two interacting modes system. Equation 3 implies that the $S(Q,\omega)$ of each mode is described by a DHO when $U(Q) = 0$.

Each data set was fitted using eq 1 with the proper scale factor K_i. To improve the robustness of the fit, an overall fitting procedure was set up in order to accurately provide both Q-dependent and Q-independent parameters by fitting all of the spectra for both instruments at the same time. The so-obtained fit was validated by performing a Bayesian analysis.[30] The resulting best-fit curves are shown in Figure 2 by red lines together with the individual inelastic components (blue lines). In panels (c) and (f), TOFTOF data are shown after subtraction of the j_1 contribution. The coupling between j_2 and j_3 introduces a deformation of the DHO line shape that is visible in Figure 2f. In particular, j_2 shows a double-peaked structure.

Figure 3a shows the dispersion curves obtained by plotting the parameters $\omega_{Q\,j_1}$ and $\Omega_{2,3}(Q)$, where

$$\Omega^2_{2,3}(Q) = \frac{\omega^2_{Q\,j_2} + \omega^2_{Q\,j_3} \pm \sqrt{(\omega^2_{Q\,j_2} - \omega^2_{Q\,j_3})^2 + 4|U(Q)|^2}}{2}$$

The majority of the inelastic intensity (about ~75%) is contributed by the branch j_1, which shows a dispersion characterized by a maximum at $Q_m \approx 1$ Å^{-1},[22] followed by a decreasing trend for $Q > Q_m$. This can be identified as a longitudinal acoustic behavior. Figure 3a reports also the Brillouin light scattering (BLS) longitudinal and transverse sound velocities from ref 21, $v_L^0 = 1740$ m/s and $v_T^0 = 940$ m/s, respectively. Using the present data, a longitudinal sound velocity of $v_L^\infty = 2590 \pm 80$ m/s is obtained, a value ~50% higher than v_L^0.

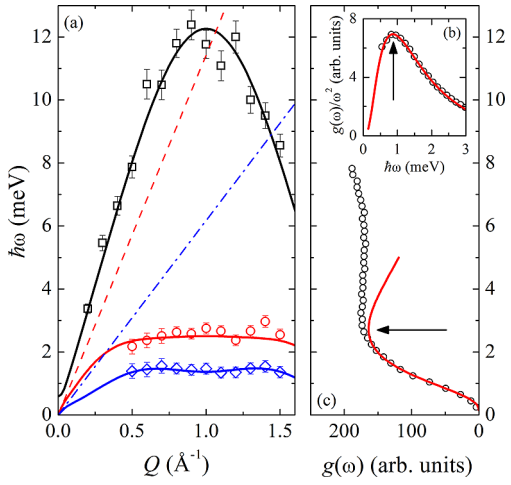

Figure 3. (a) Dispersion curves for j_1 (black open squares), j_2 (red open circles), and j_3 (blue open diamonds). Solid lines represent the curves obtained by fitting the dynamical matrix (see text). The longitudinal (red dashed line) and transverse (blue dashed−dotted line) BLS sound velocities are also reported.[21] (b) Reduced density of states $g(\omega)/\omega^2$ (black open circles); the arrow marks the BP position E_{BP} obtained by fitting a log-normal function $f(\omega)$ to the data (red line). (c) Vibrational density of states $g(\omega)$ (black open circles); the red line is $f(\omega)\omega^2$. The arrow highlights the position of the BP in $g(\omega)$, that is, $\tilde{E}_{BP}$ (see text).

The remaining ~25% of the inelastic intensity is represented by j_2 and j_3, which have an almost Q-independent energy. The intensity of these modes decreases when Q is reduced, thus suggesting either a transverse or an optic nature.

Our analysis enhances the presence in $SiSe_2$ of a rich pattern of low-energy vibrations, even more complex than that observed in previous and accurate investigations in other systems,[15,16,19] where two modes were detected. A complete understanding of the $SiSe_2$ dynamics, and possibly of other systems, needs identification of the modes' character. To this purpose, we compare the dynamical matrix $\mathbb{D}(Q)$ of *three* interacting modes to the dispersion relation of Figure 3a. In fact, as we are going to take into account also the BLS frequency of the acoustic modes, we access a Q region where the interaction of j_1 has now to be considered. Accordingly, $\mathbb{D}_{\alpha\alpha}(Q) = \omega^2 - \omega^2_{Q\,j_\alpha}$, and the off-diagonal terms have the same functional form as $U(Q)$ with appropriate parameters. A complete and consistent account of the experimental results is obtained when $\mathbb{D}_{1,2}(Q) = 0$, $\mathbb{D}_{2,3}(Q) = U(Q)$, and $\mathbb{D}_{1,3}(Q) = U_{1,3}Q\exp[-R^2_{1,3}Q^2]$ is fitted to the data in Figure 3a. In this model, at high Q, j_1 and j_2 have a longitudinal and transverse acoustic character, respectively, whereas j_3 has an optic-like character. We note that this scheme perfectly accounts for the low-frequency sound velocity through the interaction between the two acoustic modes and the optic-like one. Moreover, the model, showing the presence of two acoustic modes, gives further strength to the identification of the two modes already observed in other systems.[15,16,19] On the other hand, the observation of an optic-like excitation might be a peculiar characteristic of $SiSe_2$ because it was not identified in previous high-resolution studies.

Finally, it is worth mentioning the relation between the BP and the excitation spectrum. As shown in Figure 3c, the BP energy in $SiSe_2$ is $E_{BP} = 0.88 \pm 0.05$ meV, obtained by fitting a log-normal function to the reduced density of states $g(\omega)/\omega^2$.[31] In the vibrational density of states, the BP maximum modes are located at $\tilde{E}_{BP} = 2.7 \pm 0.2$ meV, which has a good correspondence to the branch j_2 identified as transverse acoustic. This further supports the link between BP and transverse acoustic modes.[4,8,14]

EXPERIMENTAL METHODS

Silicon selenium glasses Si_xSe_{1-x} can be produced over a wide interval of concentrations by melt quenching.[32] In the present case, we chose $x = 0.365$, a value close to the stoichiometric formula $SiSe_2$ and lying in a region where the glassy phase can be efficiently obtained.[32,33] The sample was prepared starting from pure Si and Se powders (Aldrich, Si 99.999% and Se 99.99%). Silicon diselenide is strongly reactive in a normal atmosphere; therefore, the sample was prepared under a controlled argon atmosphere by mixing the powders at the nominal composition inside of a quartz tube. The sealed tubes were then heated at 1320 K for 96 h and finally quenched into liquid water, thus obtaining a yellowish glass.[32] Neutron

dx.doi.org/10.1021/jz400232c | J. Phys. Chem. Lett. 2013, 4, 1143−1147

scattering experiments were carried out at room temperature. The neutron samples were fine $SiSe_2$ powders produced by grinding the bulk glass under a controlled inert atmosphere and loaded into vacuum-sealed aluminum cells (a flat cell for BRISP, h = 30 mm v = 30 mm, and t = 10 mm, and a hollow cylinder for TOFTOF, d_o = 25 mm d_i = 18 mm, and h = 40 mm).

We performed two different experiments at the spectrometers BRISP (Institut Laue Langevin, Grenoble, France),[25,26] and TOFTOF (FRM-II, Münich, Germany).[27] Using an incident energy of 83.6 meV, BRISP is able to investigate a wide energy range with a resolution of 3.1 meV. Conversely, TOFTOF can be set to span a narrow region close to the elastic line. With an incident energy of 3.27 meV and a chopper speed of 12000 rpm, a resolution of 150 μeV is obtained. The ($\hbar\omega$,Q) kinematic regions investigated and the instrumental resolutions are reported in Figure 1. The measured intensities were reduced by carefully subtracting the contributions of the background and empty cell and corrected for multiple scattering effects by using a Monte Carlo simulation[34,35] that provides also the calculated transmission coefficients.

AUTHOR INFORMATION

Corresponding Author

*E-mail: marco.zanatta@fisica.unipg.it.

Notes

The authors declare no competing financial interest.

ACKNOWLEDGMENTS

We Acknowledge C. Armellini, C. Corradi, and R. Dal Maschio for help in the sample preparation and T. Unruh and J. Ringe for assistance during the measurements at TOFTOF. The FRM-II experiment was financed through the NMI3 access program.

REFERENCES

(1) Buchenau, U.; Nücker, N.; Dianoux, A. J. Neutron Scattering Study of the Low-Frequency Vibrations in Vitreous Silica. *Phys. Rev. Lett.* **1984**, *53*, 2316−2319.

(2) Doster, W.; Cusack, S.; Petry, W. Dynamical Transition of Myoglobin Revealed by Inelastic Neutron Scattering Nature. *Nature* **1989**, *337*, 754−756.

(3) Frick, B.; Richter, D. The Microscopic Basis of the Glass Transition in Polymers from Neutron Scattering Studies. *Science* **1995**, *267*, 1939−1945.

(4) Taraskin, S. N.; Loh, Y. L.; Natarajan, G.; Elliott, S. R. Origin of the Boson Peak in Systems with Lattice Disorder. *Phys. Rev. Lett.* **1995**, *86*, 1255−1258.

(5) Shintani, H.; Tanaka, H. Universal Link Between the Boson Peak and Transverse Phonons in Glass. *Nat. Mater.* **2008**, *7*, 870−877.

(6) Duval, E.; Mermet, A.; Saviot, L. Boson Peak and Hybridization of Acoustic Modes with Vibrations of Nanometric Heterogeneities in Glasses. *Phys. Rev. B* **2007**, *75*, 024201.

(7) Rufflé, B.; Parshin, D. A.; Courtens, E.; Vacher, R. Boson Peak and its Relation to Acoustic Attenuation in Glasses. *Phys. Rev. Lett.* **2008**, *100*, 015501.

(8) Chumakov, A. I.; et al. Equivalence of the Boson Peak in Glasses to the Transverse Acoustic van Hove Singularity in Crystals. *Phys. Rev. Lett.* **2011**, *106*, 225501.

(9) Zanatta, M.; Baldi, G.; Caponi, S.; Fontana, A.; Petrillo, C.; Rossi, F.; Sacchetti, F. Debye to Non-Debye Scaling of the Boson Peak Dynamics: Critical Behavior and Local Disorder in Vitreous Germania. *J. Chem. Phys.* **2011**, *135*, 174506.

(10) Elliott, S. R. Medium-Range Structural Order in Covalent Amorphous Solids. *Nature* **1991**, *354*, 445−452.

(11) Monaco, G.; Mossa, S. Anomalous Properties of the Acoustic Excitations in Glasses on the Mesoscopic Length Scale. *Proc. Natl. Acad. Sci. U.S.A.* **2009**, *106*, 16907−16912.

(12) Monaco, G.; Giordano, V. Breakdown of the Debye Approximation for the Acoustic Modes with Nanometric Wavelengths in Glasses. *Proc. Natl. Acad. Sci. U.S.A.* **2008**, *128*, 244507−569.

(13) Pilla, O.; Angelani, L.; Fontana, A.; Gonsalves, J.; Ruocco, G. Structural and Dynamical Consequences of Density Variation in Vitreous Silica. *J. Phys.: Condens. Matter* **2003**, *15*, S995.

(14) Pilla, O.; Caponi, S.; Fontana, A.; Gonsalves, J. R.; Montagna, M.; Rossi, F.; Viliani, G.; Angelani, L.; Ruocco, G.; Monaco, G.; Sette, F. The Low Energy Excess of Vibrational States in v-SiO_2: The Role of Transverse Dynamics. *J. Phys.: Condens. Matter* **2004**, *16*, 8519.

(15) Ruzicka, B.; Scopigno, T.; Caponi, S.; Fontana, A.; Pilla, O.; Giura, P.; Monaco, G.; Pontecorvo, E.; Ruocco, G.; Sette, F. Evidence of Anomalous Dispersion of the Generalized Sound Velocity in Glasses. *Phys. Rev. B* **2004**, *69*, 100201.

(16) Bove, L. E.; Fabiani, E.; Fontana, A.; Paoletti, F.; Petrillo, C.; Pilla, O.; Bento, I. C. V. Brillouin Neutron Scattering of v-GeO_2. *Europhys. Lett.* **2005**, *71*, 563−569.

(17) Fabiani, E.; Fontana, A.; Buchenau, U. Neutron Scattering Study of the Vibrations in Vitreous Silica and Germania. *J. Chem. Phys.* **2008**, *71*, 563−569.

(18) Baldi, G.; Giordano, V.; Monaco, G. Elastic Anomalies at Terahertz Frequencies and Excess Density of Vibrational States in Silica Glass. *Phys. Rev. B* **2011**, *83*, 174203.

(19) Orsingher, L.; Baldi, G.; Fontana, A.; Bove, L. E.; Unruh, T.; Orecchini, A.; Petrillo, C.; Violini, N.; Sacchetti, F. High-Frequency Dynamics of Vitreous $GeSe_2$. *Phys. Rev. B* **2010**, *82*, 115201.

(20) Violini, N.; Orecchini, A.; Paciaroni, A.; Petrillo, C.; Sacchetti, F. Neutron Scattering Investigation of High-Frequency Dynamics in Glassy Glucose. *Phys. Rev. B* **2012**, *85*, 134204.

(21) Bhadra, R.; Susman, S.; Volin, K. J.; Grimsditch, M. Elastic Properties of Si_xSe_{1-x} Glasses. *Phys. Rev. B* **1989**, *39*, 1378−1380.

(22) Johnson, R.; Price, D.; Susman, S.; Arai, M.; Morrison, T.; Shenoy, G. The Structure of Silicon−Selenium Glasses: I. Short-Range Order. *J. Non-Cryst. Solids* **1986**, *83*, 251−271.

(23) Gladden, L. F.; Elliott, S. R. Computer-Generated Models of *a*-$SiSe_2$: Evidence for a Glass Exhibiting Medium-Range Order. *Phys. Rev. Lett.* **1987**, *59*, 908−911.

(24) Celino, M.; Massobrio, C. Origin of Network Connectivity and Structural Units in Amorphous $SiSe_2$. *Phys. Rev. Lett.* **2003**, *90*, 125502.

(25) Orecchini, A.; Paciaroni, A.; Francesco, A. D.; Sani, L.; Marconi, M.; Laloni, A.; Guarini, E.; Formisano, F.; Petrillo, C.; Sacchetti, F. Brillouin Spectroscopy of Protein Hydration Water: New Experimental Potentialities Opened Up by the Thermal Neutron Spectrometer BRISP. *Meas. Sci. Technol.* **2008**, *19*, 034026.

(26) Aisa, D.; et al. The Development of the BRISP Spectrometer at the Institut Laue−Langevin. *Nucl. Instrum. Methods Phys. Res., Sect. A* **2005**, *544*, 620−642.

(27) Unruh, T.; Neuhaus, J.; Petry, W. The High-Resolution Time-of-Flight Spectrometer TOFTOF. *Nucl. Instrum. Methods Phys. Res., Sect. A* **2007**, *580*, 1414−1422.

(28) Zubarev, D. N. Double-Time Green Functions in Statistical Physics. *Sov. Phys. Usp.* **1960**, *3*, 320.

(29) Lovesey, S. W. *Theory of Neutron Scattering from Condensed Matter*, 2nd ed.; Oxford University Press: New York, 1986; Vol. *I*.

(30) Sivia, D. *Data Analysis: A Bayesian Tutorial*, 1st ed.; Oxford University Press: New York, 1996.

(31) Malinovsky, V. K.; Novikov, V. N.; Sokolov, A. P. Log-Normal Spectrum of Low-Energy Vibrational Excitations in Glasses. *Phys. Lett. A* **1991**, *153*, 63−66.

(32) Johnson, R.; Susman, S.; McMillan, J.; Volin, K. Preparation and Characterization of Si_xSe_{1-x} Glasses and Determination of the Equilibrium Phase Diagram. *Mater. Res. Bull.* **1986**, *21*, 41−47.

(33) Arai, M.; Price, D. L.; Susman, S.; Volin, K. J.; Walter, U. Network Dynamics of Chalcogenide Glasses. II. Silicon Diselenide. *Phys. Rev. B* **1988**, *37*, 4240−4245.

(34) Petrillo, C.; Sacchetti, F. Analysis of Neutron Diffraction Data in the Case of High-Scattering Cells. II. Complex Cylindrical Cells. *Acta Crystallogr., Sect. A* **1992**, *48*, 508−515.
(35) Petrillo, C.; Sacchetti, F. Analysis of Neutron Diffraction Data in the Case of High-Scattering Cells. *Acta Crystallogr., Sect. A* **1990**, *46*, 440−449.